Soft Matter

ARTICLE TYPE

Cite this: DOI: 00.0000/xxxxxxxxxx

A phase field model for dynamic simulations of reactive blending of polymers†

Mukul D. Tikekar,[a], Kris T. Delaney,[a], Michael C. Villet,[b], Douglas R. Tree,[c], and Glenn H. Fredrickson*[a]

Received Date
Accepted Date

DOI: 00.0000/xxxxxxxxxx

A facile way to generate compatibilized blends of immiscible polymers is through reactive blending of end-functionalized homopolymers. The reaction may be reversible or irreversible depending on the end-groups and is affected by the immiscibility and transport of the reactant homopolymers and the compatibilizing copolymer product. Here we describe a phase-field framework to model the combined dynamics of reaction kinetics, diffusion, and multi-component thermodynamics on the evolution of the microstructure and reaction rate in reactive blending. A density functional with no fitting parameters, which is obtained by adapting a framework of Uneyama and Doi and qualitatively agrees with self-consistent field theory, is used in a diffusive dynamics model. For a symmetric mixture of equal-length reactive polymers mixed in equal proportions, we find that depending on the Flory χ parameter, the microstructure of an irreversibly reacting blend progresses through a rich evolution of morphologies, including from two-phase coexistence to a homogeneous mixture, or a two-phase to three-phase coexistence transitioning to a homogeneous blend or a lamellar copolymer. The emergence of a three-phase region at high χ leads to a previously unreported reaction rate scaling. For a reversible reaction, we find that the equilibrium composition is a function of both the equilibrium constant for the reaction and the χ parameter. We demonstrate that phase-field models are an effective way to understand the complex interplay of thermodynamic and kinetic effects in a reacting polymer blend.

1 Introduction

Reactive blending is an industrially important process for compatibilizing blends of immiscible polymers, resulting in composites with enhanced properties[1–3]. In this process, two or more polymers with reactive groups are typically mixed in an extruder to generate *in situ* copolymer at their domain interfaces, creating an emulsified alloy that often has superior properties to a physical blend wherein a copolymer is separately added to a homopolymer mixture[4,5]. The reaction may be one of end-coupling where end-functional polymers link together to form a diblock copolymer[6], or one of homopolymers chemically attacking each other (as in trans-esterification reactions) to generate a range of sequence-scrambled linear or graft copolymers[7]. In any case, the copolymer acts as a compatibilizer that improves adhesion and reduces the interfacial tension between the homopolymer phases. This effect may be further enhanced if the interfacial copolymer is entangled with the bulk homopolymers[8]. In the presence of extruder flows, the copolymer crowds the interfaces of droplets even at small concentrations, suppressing coalescence and yielding finer dispersions[9–11]. In extreme situations, the process can generate so much copolymer that the interface starts to roughen spontaneously[12,13]. The combined effects of thermodynamics of multi-component self-assembling systems, kinetics of the coupling reaction, diffusion, and convection by flow create a complex problem of deep fundamental and practical interest.

Even physical blends of two homopolymers (types A and B) and a linear AB diblock copolymer show a rich diversity of microstructures ranging from macrophases of homopolymers to copolymer controlled microphases such as lamellae, hexagonally packed cylinders, or cubic arrangements of spheres, to co-continuous morphologies depending on the diblock volume fraction ϕ_D[3,14–19]. Using the random phase approximation (RPA), Broseta and Fredrickson[20] showed that the phase behavior of this system undergoes a transition from the disordered phase to macrophases or microphases depending on the relative proportions of the three components and the incompatibility of the two monomer species, quantified by a Flory interaction param-

[a] *Materials Research Laboratory, University of California, Santa Barbara, United States. Fax: +1-805-893-8797; Tel: +1-805-893-8308; E-mail: ghf@mrl.ucsb.edu*
[b] *Covestro Resins B.V., Geleen, The Netherlands.*
[c] *Chemical Engineering Department, Brigham Young University, Provo, United States.*
† Electronic Supplementary Information (ESI) available: [details of any supplementary information available should be included here]. See DOI: 10.1039/cXsm00000x/

eter χ. Specifically, the isopleth plane (χ vs. ϕ_D) corresponding to equal amounts of equal-length A and B homopolymers, mixed with a compositionally symmetric AB diblock at volume fraction ϕ_D, contains a mean-field Lifshitz point, where disordered (DIS), lamellar microphase (LAM), and two macrophases rich in A and B homopolymers (2φ) coexist. Janert and Schick [15] used self-consistent field theory to show that for symmetric blends at large χ, the phase diagram contains a three phase (3φ) region in which two homopolymer-rich phases coexist with a LAM phase. This phase behavior is altered slightly when the diblock is generated by a reversible reaction and the location of the Lifshitz point depends on the equilibrium constant of the reaction. The system also exhibits re-entrant thermal transitions for the LAM and DIS states [21].

When the copolymer is generated by a reaction in an A-B bilayer geometry without external flow, the temporal variation of the microstructure and composition of the system are determined by the reaction kinetics, which are restricted to the interfacial manifold. Kinetics measurements in polystyrene (PS) and polymethyl-methacrylate (PMMA) blends with reactive end groups suggested that the reaction rate is strongly controlled by the diffusion of the polymers to and within the interfacial region [22,23]. O'Shaughnessy and Sawhney [11] determined that for highly reactive chains, the diffusion-limited nature of the reaction implies that the initial reaction rate depends on the chain length N_r. For unentangled polymers, chain motion is governed by Rouse dynamics and the rate constant scales as $1/\log N_r$. When the chains are long enough to be entangled, the dynamics can be described by the reptation model and the initial reaction rate scales as $1/(N_r \log N_r)$. However, once the reaction has proceeded to the point that the interface is crowded by copolymer, the copolymer presents a significant potential barrier to bringing further reactive groups together at the interface.

Fredrickson and Milner [6] extended the analysis of O'Shaughnessy and Sawhney to look at the history of the reaction rate. They found that the reaction progresses through three stages: Initially the reaction rate is kinetically controlled by diffusion of reactive units to the interface and the interfacial coverage, defined as the number of copolymer molecules per unit area, increases linearly with time t. Eventually the interface is crowded by copolymer product, leading to the reaction rate being controlled by the diffusive penetration of reactant chains through the copolymer layer. Here the interfacial coverage grows as $t^{1/2}$. At late stages, a dense copolymer brush is formed at the interface, presenting a strong potential barrier to the reactants as discussed by O'Shaughnessy and Sawhney. Here, the reaction rate drops dramatically and the interfacial coverage grows as $\log^{1/2}(t)$. Alongside the chain length dependence, the reaction rate is also affected by temperature. FTIR measurements of reaction rates in styrene-maleic anhydride (SMA) copolymer with Nylon-11 and butadiene-acrylonitrile copolymer reveal faster reactions when the chains are shorter and the temperature is higher [24]. Jones *et al.* [25] found that the reaction rate also depends on thermodynamic interactions as measured by the Flory-Huggins interaction parameter. The study notes that the rate of formation of copolymer decreases significantly with increasing χ. This is qualitatively consistent with the observed temperature dependence of the rate, since χ typically varies inversely with T; however, at the same temperature, a larger χ would also imply sharper interfaces between the homopolymers and thus a reduced manifold for the reaction.

The above theoretical work has been restricted to the simplest geometry with the interface and associated reactively-formed copolymer layer remaining planar. In practical reactive blending, this restriction is not present, so interfaces can buckle and proliferate, leading to spontaneous emulsification. Moreover, convective transport plays an important role in distributing reactants and products during the complex mixing that takes place in reactive extrusion. In this first paper in a series, we do not include convection, but relax the restriction of planar geometries and build a non-equilibrium phase field model that embeds the rich thermodynamics of a ternary A + B + AB polymer blend system. The model includes both interfacial reaction and multi-component diffusion. In a subsequent paper, we will extend the approach to include externally imposed flows and internal capillary flows.

Phase-field type models have been widely employed for the study of polymer physics [26,27] and fluid dynamics [28,29]. They are also compatible with non-equilibrium thermodynamics frameworks such as Model-B and Model-H of Hohenberg and Halperin [30] and the two-fluid model of Doi and Onuki [31], and typically require a free energy functional to construct the thermodynamic forces in the system. For complex systems, such functionals may be obtained using a number of techniques including analytical approximations built on asymptotics, [26] or systematic force-matching from self-consistent field theory [27]. Such descriptions have been used in recent years for a range of problems from shear induced demixing in polymer solutions [32–34] to membrane formation by nonsolvent-induced phase separation [35–37].

In the present work, we present a phase-field approach for determining reaction rates and morphology evolution for a binary A,B blend subject to an end-coupling reaction to form AB diblock copolymer. We begin in Section 2 with a discussion of the equilibrium phase diagram for the ternary symmetric A + B + AB system as deduced from self-consistent field theory (SCFT), a type of mean-field theory [38,39]. To simplify the parameter space, we restrict consideration to symmetric blends (equal ratios of equal-length chains) with varying amounts of symmetric diblock copolymer. In Section 3, a model is presented for the diffusive-reactive dynamics of a ternary homopolymer-copolymer blend, including reaction terms for reversibly or irreversibly generating AB diblock copolymer from an end-coupling reaction between the homopolymers. Thermodynamic forces are obtained from a free energy functional that is built using the method of Uneyama and Doi [26] and validated against the SCFT results of Section 2. The combined reaction-diffusion model is numerically solved by means of a custom pseudo-spectral code described in a previous work [35]. The results of model simulations are presented in Section 5, first studying the effect of thermodynamic and kinetic parameters on the generation rate of the copolymer in irreversible end-coupling. Based on these results, we obtain scaling relations for reaction kinetics as various phases are traversed in the phase diagram. This is followed by a look at the equilibrium properties of reversible

end-coupling as captured by the present model. The scaling relations for reaction kinetics derived earlier are used here to obtain a law of mass action in terms of an equilibrium constant and the mean concentration of copolymer formed. Finally, we briefly comment on the effect of asymmetry in blend composition and chain architecture on the reaction kinetics.

2 Equilibrium phase behavior of a symmetric homopolymer/copolymer mixture

We begin by examining the equilibrium structure of a symmetric homopolymer/copolymer blend using self consistent field theory (SCFT) in the Gibbs ensemble[40]. We consider a blend of two homopolymers A and B with chain lengths N_{Ah} and N_{Bh}, respectively, and a symmetric ($f = 0.5$) copolymer AB of length N_D, such that $N_{Ah} = N_{Bh} = N_D/2 \equiv N_r$ with N_r a reference chain length. The volume fractions of the homopolymers are taken to be equal, $\phi_{Ah} = \phi_{Bh}$, and the copolymer volume fraction ϕ_D is varied. Segmental interactions between dissimilar monomers are described by a Flory-Huggins interaction parameter χ and the melt is assumed to be incompressible. The order-disorder boundary is obtained analytically using the random phase approximation, as discussed later in Section 3.1, and matches the result of Broseta and Fredrickson.[20] A more comprehensive SCFT phase diagram is shown in Figure 1 in the χN_r-ϕ_D plane, including disordered, macrophase separated, and microphase separated regions. Along the order-disorder envelope is a Lifshitz point, shown with a black square, which delineates the tendency for macrophase vs. microphase separation.

Below the Flory critical incompatibility of $\chi N_r = 2$, the system is fully mixed and in the disordered state (DIS) at all compositions. This is due to the entropy of mixing, which overwhelms the enthalpy of mixing for such small χ values and prevents phase separation.

Between the Flory critical incompatibility and the Lifshitz χ value of $\chi_L N_r = 3$, the system exhibits two-phase liquid-liquid macrophase separation (2φ) at low copolymer concentrations. In this state an A-rich disordered phase coexists with a B-rich disordered phase, with the copolymer partitioning equally between the macrophases and to the interfaces between them. As the copolymer concentration is increased, the blend is progressively compatibilized. Above a critical copolymer concentration, the system mixes fully and forms a homogeneous DIS mixture.

Above the Lifshitz χ value, i.e. $\chi > \chi_L$, the blend continues to exhibit the 2φ structure at very low copolymer concentrations. However, above a critical concentration, the copolymer is no longer soluble in the bulk homopolymers and instead forms a third lamellar microphase (LAM) that separates the two homogeneous macrophases. In this state, the system exists in a three-phase (3φ) coexistence with an A-rich disordered phase, a B-rich disordered phase, and a lamellar microphase formed by copolymer swollen with homopolymer. As more copolymer is added to the mixture, the copolymer in the bulk disordered phases undergoes microphase separation and the system transitions into a single lamellar phase (LAM). It is interesting to note that the concentration for this transition is only weakly dependent on the incompatibility between the polymers and remains nearly at the Lifshitz concentration for the range of χ values considered. If the χ value is lower than Leibler's critical value of $\chi N_r \approx 5.25$, the pure copolymer exists in a DIS state[41]. Below this value of χ the addition of further copolymer into a homopolymer/copolymer mixture ultimately causes the blend to dissolve into a DIS structure. In comparison if $\chi N_r > 5.25$, the LAM phase persists all the way to the pure copolymer limit.

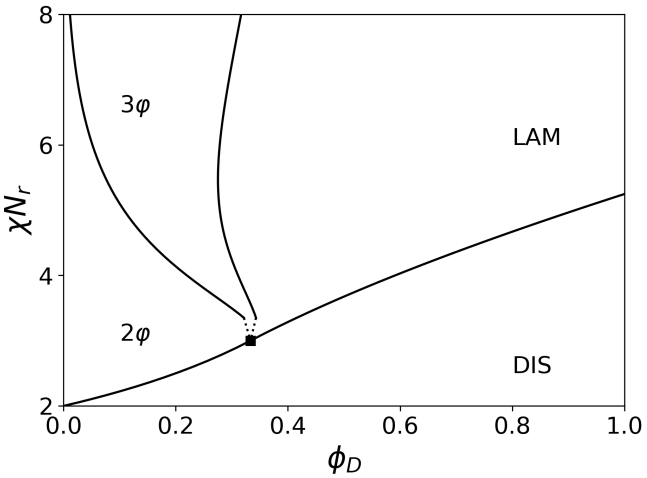

Fig. 1 Phase behavior of a symmetric blend of homopolymers A and B, and a symmetric A-B diblock copolymer obtained using self consistent field theory in the χN_r-ϕ_D plane. The system exhibits a disordered state (DIS), coexistence of two homogeneous phases (2φ), a lamellar microphase (LAM), and a three-phase coexistence (3φ) among two homopolymer-rich macrophases and a LAM microphase separating them. The Lifshitz tricritical point delineating macro- and micro-phase separated states along the order-disorder boundary[20] is shown as a square dot.

3 Model derivation

The dynamics of the system is modeled using the so-called modified Model B equations[30,35–37] based on a multi-fluid model[35], which is itself a generalization of the two-fluid formalism of Doi and Onuki[31]. The Model-B equations include diffusive transport of the various species driven by multicomponent thermodynamics and reaction dynamics. We consider a mixture of three components: two homopolymers A and B, and a linear diblock copolymer A-B with the volume fraction of the A block denoted by f. The density fields associated with the A and B segments of the diblock are resolved independently of the homopolymers to allow capture of microphase separation and to distinguish homopolymer and diblock contributions to a density pattern. We index the four types of polymer segments by an index $i = 1,\ldots,4$, corresponding respectively to segments of A homopolymer, segments of the diblock A blocks, segments of the diblock B blocks, and B homopolymer. The time evolution of the local volume fraction distributions $\phi_i(\mathbf{r},t)$ of these four components may be written as,

$$\frac{\partial \phi_i}{\partial t} = \sum_j \nabla \cdot (M_{ij} \nabla \mu_j) + R_i \qquad (1)$$

where t is time and we omit for brevity the local position dependence of all terms. M_{ij} denotes the volume-fraction-dependent relative mobilities of the species obtained from an appropriate mobility model. The thermodynamic driving forces are captured in the chemical potentials μ_i, which are defined as the variational derivative of the free-energy functional $\mathscr{F}$.

$$\mu_i = \frac{\delta \mathscr{F}}{\delta \phi_i} \tag{2}$$

The reaction-generated rates are denoted by R_i, which are modeled using an appropriate model for reaction kinetics, as described later. Finally, we assume incompressibility, which amounts to the elimination of one of the volume-fraction fields in favor of the other three. In general, for a mixture of n species, the volume fraction of the n^{th} component may be written implicitly in terms of the other components as

$$\phi_n = 1 - \sum_{j=1}^{n-1} \phi_j \tag{3}$$

Using this substitution in calculating μ_i for $i = 1,\ldots,n-1$ yields exchange chemical potentials with respect to component n. In the present situation we have $n = 4$, and homopolymer B is chosen as the implicit component.

The model can thus be completely described in terms of three elements:

1. The free-energy functional $\mathscr{F}[\{\phi_i\}]$ describes the thermodynamics of mixing including chain conformational entropy of the various species
2. The mobility model $M_{ij}[\{\phi_i\}]$ describes the dissipative couplings among the species
3. The model for reaction kinetics based on the local volume fractions $R_i[\{\phi_i\}]$ defines the kinetics of the diblock generation and decomposition processes.

The specification of each of these elements is described in the following subsections.

The Model-B equations are numerically solved using a semi-implicit time stepping scheme in a cell with spatially periodic boundary conditions and pseudo-spectral plane wave collocation as reported in a previous work.[35]

3.1 Free energy functional

We derive the free energy density functional using the procedure outlined by Uneyama and Doi[26]. This proceeds in three steps. First the random phase approximation is invoked to generate a perturbation to the free energy as a function of fluctuations in the volume fractions about a homogeneous state. The Fourier-domain response functions thus obtained are generalizations of the Debye function[41]. Next the procedure of Ohta and Kawasaki[42] is employed to convert the response functions to asymptotic, algebraic forms that can be easily Fourier-inverted. This yields a density functional for the free energy in the weak segregation limit. Finally, Uneyama and Doi[26] describe a method to generalize the functional to have improved predictive behavior in the strong segregation case of $\chi N_r \gg 1$. Using a generalization of the random phase approximation of Leibler[41], we obtain a free-energy functional in Fourier space for weak volume fraction fluctuations $\psi_i(\mathbf{k})$ about a homogeneous state with average volume fractions ϕ_{Ah}, ϕ_{Bh}, ϕ_D, and for degrees of polymerization N_{Ah}, N_{Bh}, N_D and a Flory-Huggins interaction parameter χ between monomers of type A and B,

$$\begin{aligned}\delta\mathscr{F} = \frac{1}{2}\sum_{\mathbf{k}}\Bigg[&\frac{\psi_1(\mathbf{k})\psi_1(-\mathbf{k})}{S_{11}} + \frac{\psi_4(\mathbf{k})\psi_4(-\mathbf{k})}{S_{44}} + S_{33}\frac{\psi_2(\mathbf{k})\psi_2(-\mathbf{k})}{S_{22}S_{33}-S_{23}^2} \\ &+ S_{22}\frac{\psi_3(\mathbf{k})\psi_3(-\mathbf{k})}{S_{22}S_{33}-S_{23}^2} + S_{23}\frac{\psi_2(\mathbf{k})\psi_3(-\mathbf{k})+\psi_2(-\mathbf{k})\psi_3(\mathbf{k})}{S_{22}S_{33}-S_{23}^2} \\ &+ 2\chi(\psi_1(\mathbf{k})+\psi_2(\mathbf{k}))(\psi_3(-\mathbf{k})+\psi_4(-\mathbf{k}))\Bigg]\end{aligned} \tag{4}$$

Here the relevant response functions are given as,

$$S_{11} = \phi_{Ah}N_{Ah}g(k^2R_{gAh}^2,1) \tag{5}$$

$$S_{22} = \phi_D N_D g(k^2R_{gD}^2,f) \tag{6}$$

$$S_{33} = \phi_D N_D g(k^2R_{gD}^2,1-f) \tag{7}$$

$$S_{23} = \frac{1}{2}\phi_D N_D\left(g(k^2R_{gD}^2,1) - g(k^2R_{gD}^2,f) - g(k^2R_{gD}^2,1-f)\right) \tag{8}$$

$$S_{44} = \phi_{Bh}N_{Bh}g(k^2R_{gBh}^2,1) \tag{9}$$

which uses the modified Debye function

$$g(x,f) = \frac{2}{x^2}\left(fx - 1 + \exp(-fx)\right) \tag{10}$$

and R_{gAh}, R_{gBh}, and R_{gD} are the unperturbed radii-of-gyration of the A homopolymer, B homopolymer and AB diblock components, respectively.

To obtain a phase-field type free energy functional, we invoke the Ohta and Kawasaki[42] method and approximate the response functions as a superposition of their leading asymptotic forms for $k \to 0$ and $k \to \infty$. We then invert the Fourier transform to obtain the weak segregation form of the free energy,

$$\begin{aligned}\delta\mathscr{F} = \frac{1}{2}\int d\mathbf{r}\Bigg[&\frac{\psi_1(\mathbf{r})^2}{\phi_{Ah}N_{Ah}} + \frac{\psi_4(\mathbf{r})^2}{\phi_{Bh}N_{Bh}} + \left(s(f)+\frac{1}{4}\right)\frac{\psi_2(\mathbf{r})^2}{f^2\phi_D N_D} \\ &+ \left(s(1-f)+\frac{1}{4}\right)\frac{\psi_3(\mathbf{r})^2}{(1-f)^2\phi_D N_D} - \frac{\psi_2(\mathbf{r})\psi_3(\mathbf{r})}{2f(1-f)\phi_D N_D} \\ &+ 2\chi(\psi_1(\mathbf{r})+\psi_2(\mathbf{r}))(\psi_3(\mathbf{r})+\psi_4(\mathbf{r})) \\ &+ \frac{b^2}{12}\left(\frac{|\nabla\psi_1(\mathbf{r})|^2}{\phi_{Ah}} + \frac{|\nabla\psi_4(\mathbf{r})|^2}{\phi_{Bh}} + \frac{|\nabla\psi_2(\mathbf{r})|^2}{f\phi_D} + \frac{|\nabla\psi_3(\mathbf{r})|^2}{(1-f)\phi_D}\right) \\ &+ \int d\mathbf{r}'\frac{9}{\phi_D N_D^2 b^2}G(\mathbf{r}-\mathbf{r}')\left\{\frac{\psi_2(\mathbf{r})}{f} - \frac{\psi_3(\mathbf{r})}{1-f}\right\}\left\{\frac{\psi_2(\mathbf{r}')}{f} - \frac{\psi_3(\mathbf{r}')}{1-f}\right\}\Bigg]\end{aligned} \tag{11}$$

where b is the statistical segment length, which is assumed the same for segments of all species. Following the procedure of Uneyama and Doi[26], the function $s(f)$ is determined by matching the minima in the correlation functions in Equation 11 with the corresponding functions in the full RPA expansion in Equation 4. For symmetric copolymers, we obtain $s(0.5) = 0.4015$.

The final step is to extend the free energy functional to strong segregation using the method described by Uneyama and Doi[26]. This yields a functional expressed in local volume fractions of components $\phi_i(\mathbf{r})$ rather than local fluctuations in volume fraction $\psi_i(\mathbf{r})$,

$$\mathscr{F} = \int d\mathbf{r} \Bigg[\frac{\phi_1(\mathbf{r})\log(\phi_1(\mathbf{r}))}{N_{Ah}} + \frac{\phi_4(\mathbf{r})\log(\phi_4(\mathbf{r}))}{N_{Bh}} + s(f)\frac{\phi_2(\mathbf{r})\log(\phi_2(\mathbf{r}))}{fN_D} + s(1-f)\frac{\phi_3(\mathbf{r})\log(\phi_3(\mathbf{r}))}{(1-f)N_D} - \frac{\sqrt{\phi_2(\mathbf{r})\phi_3(\mathbf{r})}}{\sqrt{f(1-f)}N_D} + \chi(\phi_1(\mathbf{r})+\phi_2(\mathbf{r}))(\phi_3(\mathbf{r})+\phi_4(\mathbf{r})) + \frac{b^2}{24}\left(\frac{|\nabla\phi_1(\mathbf{r})|^2}{\phi_1} + \frac{|\nabla\phi_4(\mathbf{r})|^2}{\phi_4} + \frac{|\nabla\phi_2(\mathbf{r})|^2}{\phi_2} + \frac{|\nabla\phi_3(\mathbf{r})|^2}{\phi_3}\right) + \int d\mathbf{r}' \frac{9\,G(\mathbf{r}-\mathbf{r}')}{2(\phi_2+\phi_3)N_D^2 b^2}\left\{\frac{\phi_2(\mathbf{r})}{f} - \frac{\phi_3(\mathbf{r})}{1-f}\right\}\left\{\frac{\phi_2(\mathbf{r}')}{f} - \frac{\phi_3(\mathbf{r}')}{1-f}\right\}\Bigg] \tag{12}$$

Here, the overbars denote spatial averages. $G(\mathbf{r}-\mathbf{r}')$ is the Green function of the Poisson equation obtained from the solution of $\nabla^2 G(\mathbf{r}-\mathbf{r}') = -\delta(\mathbf{r}-\mathbf{r}')$.

The first four terms in the above free energy functional are of the form $\phi_i\log(\phi_i)$ and represent the translational entropies of the four components. However, the 2nd and 3rd components are connected into diblocks, so the $s(f)$ and $s(1-f)$ factors in the third and fourth terms and the fifth term proportional to $\sqrt{\phi_2\phi_3}$ correct the overcounting of diblock translational degrees of freedom. The sixth term is the enthalpic interaction among the various components based on Flory-Huggins theory. This is followed by a sum of terms that are proportional to $|\nabla\phi_i|^2$, which are called "square gradient" terms. These terms penalize the creation of interfaces and reflect a loss of chain conformational entropy at such interfaces. The final term contains the Green function mentioned earlier. This term is attributed to the covalent bonding between the two parts of the diblock copolymer and represents long range interactions between the two blocks. This prevents macrophase separation of the pure diblock, leading instead to microphase separation at sufficiently large χ values. The length scale for microphase separation, typically of order the scale of R_{gD}, is set by the balance of the Green function term, which penalizes long microdomain periods and the square gradient terms, which penalize short periods.

Numerical optimization of the free energy functional of equation 12 has been shown to semi-quantitatively capture the phase behavior of a pure diblock copolymer melt, as well as the equilibrium structure of an A and B homopolymer and A-B diblock ternary blend, both comparisons made against the "gold standard" of self-consistent field theory[26]. In the weak segregation limit, which is the regime of present investigation, free energy optimization also shows quantitative agreement with self-consistent field theory as shown in Figure 2. In the subsequent discussion, we restrict ourselves to symmetric diblocks for which $s(0.5) = 0.4015$.

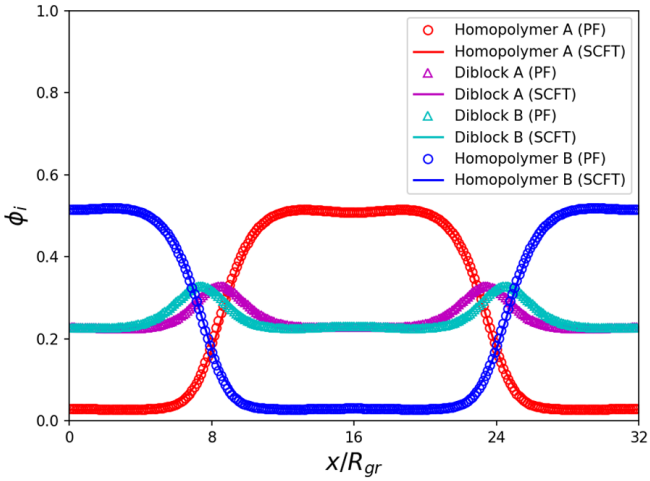

Fig. 2 Comparison between equilibrium distributions obtained using the Model-B equations to optimize the energy functional $\mathscr{F}$ (phase field, PF) and by self-consistent field theory (SCFT), showing the agreement between the two models. The composition of the system being studied is: $<\phi_1>=<\phi_4>=0.25$, $f=0.5$, $N_{Ah}=N_{Bh}=N_D=N_r$, $\chi N_r = 6$

3.2 Rouse mobilities

The mobilities are obtained as functions of local volume fractions using the Rouse model. Assuming incompressibility, the volume fraction of one of the components is written in terms of the others as shown in Equation 3. The Rouse mobilities are derived based on exchange chemical potentials as presented in a previous work[35], giving

$$M_{ij} = \frac{1}{\zeta_0}\phi_i(1-\phi_i) \qquad i=j$$
$$= -\frac{1}{\zeta_0}\phi_i\phi_j \qquad i\neq j \tag{13}$$

where ζ_0 is a segment friction coefficient.

3.3 Reaction model

Two simultaneous reactions are considered here: a diblock-generating forward reaction and a diblock-consuming reverse reaction, as illustrated in Figure 3a. The forward reaction is an end-coupling reaction between one A and one B homopolymer to generate one diblock molecule, while the reverse reaction is the spontaneous decomposition of a diblock chain to generate one chain of each homopolymer. The kinetics of the forward and reverse reactions are obtained separately by tracking the reactive groups on the polymers as shown in Figure 3b.

For the diblock-generating forward reaction, the reaction rate

between the reactive end-groups on the homopolymers, denoted by R_f, is given as a second-order reaction,

$$R_f = k_f \phi_{1^*} \phi_{4^*} \tag{14}$$

where the asterisk denotes a dilution effect because only the end monomer of each homopolymer is reactive. In contrast, the reverse reaction that causes the diblock molecules to spontaneously break up is modeled as a first-order reaction

$$R_b = k_b \phi_{D^*} \tag{15}$$

Assuming that the reactive groups are homogeneously distributed in space within the individual components, we can write

$$\phi_{1^*} = \frac{\phi_1}{N_{Ah}}$$

$$\phi_{4^*} = \frac{\phi_4}{N_{Bh}}$$

$$\phi_{D^*} = \frac{\phi_2 + \phi_3}{N_D} \tag{16}$$

where $N_D = N_{Ah} + N_{Bh}$ since the diblock is assembled from the homopolymers. Every instance of the forward reaction changes all monomers in one chain each of homopolymers A and B to monomers of the diblock's A and B blocks, respectively. Likewise, each instance of the backward reaction changes all the monomers of the corresponding block of the diblock to the respective homopolymer. By conservation of mass, the total number of monomers of each species A and B remain unchanged. This gives,

$$R_1 = -R_2 = -R_f N_{Ah} + R_b N_D \frac{\phi_2}{\phi_2 + \phi_3} = -k_f \frac{\phi_1 \phi_4}{N_{Bh}} + k_b \phi_2$$

$$R_4 = -R_3 = -R_f N_{Bh} + R_b N_D \frac{\phi_3}{\phi_2 + \phi_3} = -k_f \frac{\phi_1 \phi_4}{N_{Ah}} + k_b \phi_3 \tag{17}$$

which are the reaction rates in the model equations. It is important to note that the rates are dependent on the index of polymerization of the homopolymers. This is because at constant monomer density, changing the lengths of the homopolymers affects the relative concentration of reactive groups. Specifically, the forward reaction requires a reactive end-group each of homopolymers A and B to come together. These groups are distributed in space with proportions of $1/N_{Ah}$ and $1/N_{Bh}$ of the respective volume fractions, giving a net reaction probability of $1/(N_{Ah}N_{Bh})$. With one instance of reaction, N_{Ah} monomers of homopolymer A, and N_{Bh} monomers of homopolymer B are converted to diblock monomers respectively. Consequently, the volume fractions of homopolymers A and B decrease with a proportionalities of $1/N_{Bh}$ and $1/N_{Ah}$ respectively, as is reflected in the terms with k_f in the rate equation (17). If the homopolymers are of different lengths, this means that the longer polymer is consumed more quickly in volumetric terms than the shorter polymer, simply because each reaction converts a proportionally larger number of monomers of the longer polymer.

Likewise, the reverse reaction occurs with a probability of $1/N_D$ in space, proportional to the volume fraction of the diblock, and

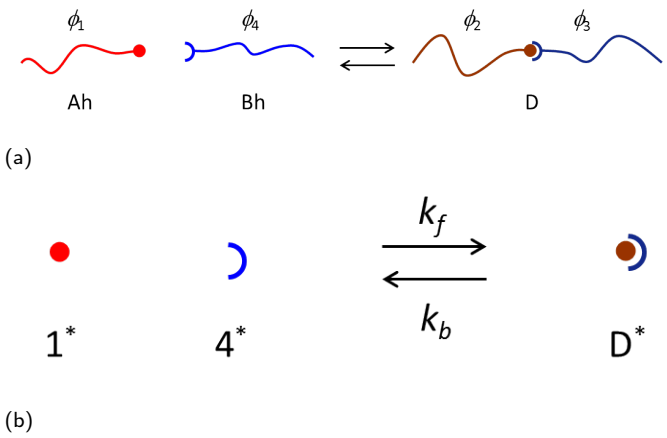

Fig. 3 Model of the reversible reaction between (a) the polymers and (b) the reactive end groups used for determining the kinetics. The reaction kinetics equations are developed in the text.

generates fN_D and $(1-f)N_D$ monomers of homopolymers A and B, respectively, which is also seen in the terms with k_b in the rate equation (17).

4 Nondimensional analysis

The above equations are solved in a nondimensional form. The chain lengths of polymers N_{Ah}, N_{Bh}, N_D are scaled with a reference chain length N_r. The choice of the characteristic length scale is important since it also determines the time scale and hence the nondimensionalization of the problem. A wide range of length scales is available, such as the radii of gyration of the homopolymers and diblock, the thickness of the interface between the homopolymers at equilibrium, the size of the homopolymer domains, and the size of the simulation box, some of which depend on the composition and properties of the system. To keep the relevance of the study as broad as possible, we select the characteristic length scale from the reference polymer length as $R_{gr} = b\sqrt{N_r/6}$. The self diffusion coefficient in a melt of unentangled Rouse reference chains is given by,

$$D = \frac{k_B T}{N_r \zeta_0} \tag{18}$$

Here k_B is the Boltzmann constant and T is temperature. This gives the characteristic time scale as the Rouse time,

$$\tau = \frac{R_{gr}^2}{D} = \frac{N_r^2 b^2 \zeta_0}{6 k_B T} \tag{19}$$

Two Damkohler numbers are obtained by nondimensionalizing the forward and backward rate constants with the diffusive (Rouse) time scale. Their ratio is the reaction equilibrium constant. For presenting the results, we select the forward reaction Damkohler number and the equilibrium constant, defined as,

$$Da_f = \frac{k_f N_r^2 b^2 \zeta_0}{6 k_B T} \tag{20}$$

$$K = \frac{k_f}{k_b} \tag{21}$$

It is worth noting that the forward and reverse reaction rates have different dependencies on chain lengths. For fully miscible blends, this means that the equilibrium composition of the system depends on both the equilibrium constant and the chain lengths as,

$$K\left(\frac{1}{N_{Ah}}+\frac{1}{N_{Bh}}\right)=\frac{\phi_2+\phi_3}{\phi_1\phi_4} \tag{22}$$

The left hand side of this equation can be viewed as an effective equilibrium constant $K_{\text{eff}}(T,N_r)$ that is both temperature and chain-length dependent.

5 Results

We start by looking at an irreversibly reacting symmetric homopolymer blend in a 1D configuration. This reaction is obtained by setting the backward rate constant $k_b=0$ and corresponds to the case where the equilibrium constant $K=\infty$. Two homopolymers of identical lengths $N_{Ah}=N_{Bh}=N_r$ and in equal proportions are initialized in a macrophase separated profile with a diffuse interface between them as shown in Figure 4a. The reaction and transport are turned on at $t=0$, allowing for the creation of diblock at the interfaces and diffusive transport of all three species.

This is then followed by a study of reversible end-linking, where the copolymer formed as a result of end-linking between the homopolymers can spontaneously dissociate back into the reactants. Here we will focus on the time evolution to the steady state composition of the system as a function of the thermodynamic and kinetic parameters.

5.1 Irreversible end-coupling

Figure 4 shows a time lapse of volume fraction distributions of the various species for $\chi N_r=3$ and $Da_f=0.3$. The homopolymers react at the interface and generate a diblock copolymer layer. At this stage the reaction is kinetically limited. The copolymer generation is fast enough that the newly formed chains do not have sufficient time to stretch at the interface, and the concentrations of the two blocks are nearly identical. Over time, a dense copolymer brush builds up at the interface and limits the reaction by reducing contact between the homopolymers. The copolymer also compatibilizes the homopolymers and creates a more diffuse interface. Continuing the reaction further requires that the homopolymer diffuse through the copolymer brush, while the copolymer itself diffuses out into the bulk homopolymer domains. The reaction is limited by this diffusion through barriers. This picture is qualitatively consistent with that of Fredrickson and Milner [6]. Eventually the homopolymer gets depleted from the system and the reaction is complete.

We study the kinetics in further depth in Figure 5a which shows the relation between the diblock generation rate, $\left\langle \dot{\phi}_D \right\rangle$, against the mean diblock volume fraction, $\langle\phi_D\rangle$, which is analogous to the reaction rate against the extent of the reaction. Here the angular brackets denote spatial averaging. In Figure 5b, the interfacial excess z^*, defined as [2]

$$z^*=\int(\phi_D(x)-\phi_{D,\infty})dx, \tag{23}$$

is shown as a function of time, where $\phi_{D,\infty}$ is the volume fraction of the diblock deep in the bulk-like regions of the homopolymer domains. The progress of the reaction through the two regimes is clearly seen in both plots.

During the initial regime, the diblock is generated only in the diffuse interface of thickness ξ. Consequently, a thicker interface proportionally produces more copolymer and the concentration of the diblock in the bulk homopolymer domains remains low. The volume-averaged reaction rate scales inversely with the system size L as $k_f\xi/L$. This is also reflected in the interfacial excess which rises linearly with time at a rate of $k_f\xi$, consistent with O'Shaughnessy and Sawhney [11]. If the system is initialized as a homopolymer blend at equilibrium in the Helfand-Tagami limit ($\chi N_r\to\infty$), the growth rate of the interfacial excess will then be $k_f b/\sqrt{6\chi}$ and the reaction rate will be $k_f b/(L\sqrt{6\chi})$.

As the interface becomes saturated with diblock, the copolymer needs to diffuse out into the bulk homopolymer domains for the reaction to continue and the reaction rate drops dramatically as a result. The rate of change of mean copolymer concentration scales as $D_H^\xi/(L\xi)$. Here D_H^ξ is the diffusivity of the homopolymer in the diblock. D_H^ξ decreases with increasing χN_r due to the stronger enthalpic repulsion between the homopolymer and the opposite block of the copolymer. The inverse relation with system size persists here since the copolymer is still generated within the interfacial layer. Eventually, the copolymer diffuses into the bulk homopolymer to achieve binodal composition. The bulk copolymer concentration $\phi_{D,\infty}$ rises and the interfacial excess, by definition, decreases. The interfacial excess peaks at time $t^*\sim L^2/D_D^\infty$ signifying that the copolymer has migrated into the bulk homopolymer. Here D_D^∞ is the diffusivity of the copolymer in the bulk homopolymer. This last stage is likely not accessible in experiments, where the system size is very large, and the typical large χN_r causes the diffusivity of the diblock to be very low, resulting in a long time required for complete diffusion.

For incompatibilities larger than the Lifshitz value $\chi>\chi_L$, the system can undergo microphase separation at higher copolymer content. This is reflected in the transient states while the dynamics of the concentration evolution retains its interfacial-brush-limited nature. Figure 6 shows a time lapse of concentration evolution for the various species for $\chi N_r=6$. The starting distribution is the same as in the previous case. As before, a copolymer brush forms at the interface of the two homopolymers and slows the progress of the reaction. However as the amount of copolymer increases, the system enters the three-phase (3φ) regime. The copolymer at the interface separates into a third LAM phase, entraining homopolymer in its lamellae. These pockets of homopolymer act as "micro-reactors", with the homopolymers reacting across adjacent lamellae. The reaction rate at this stage is not limited by diffusion of the homopolymer across the entire brush, but rather kinetically over the sizes of the lamellae and scales as $k_f L_{\text{LAM}}(1-\phi_{D,\text{LAM}})^2/L$. Here L_{LAM} and $\phi_{D,\text{LAM}}$ are the thickness and the copolymer concentration of the LAM phase. The copolymer thus formed further expands the interfacial brush, shrinking the bulk homopolymer domains. Additional homopolymer is entrained into the copolymer as the reaction progresses. At very

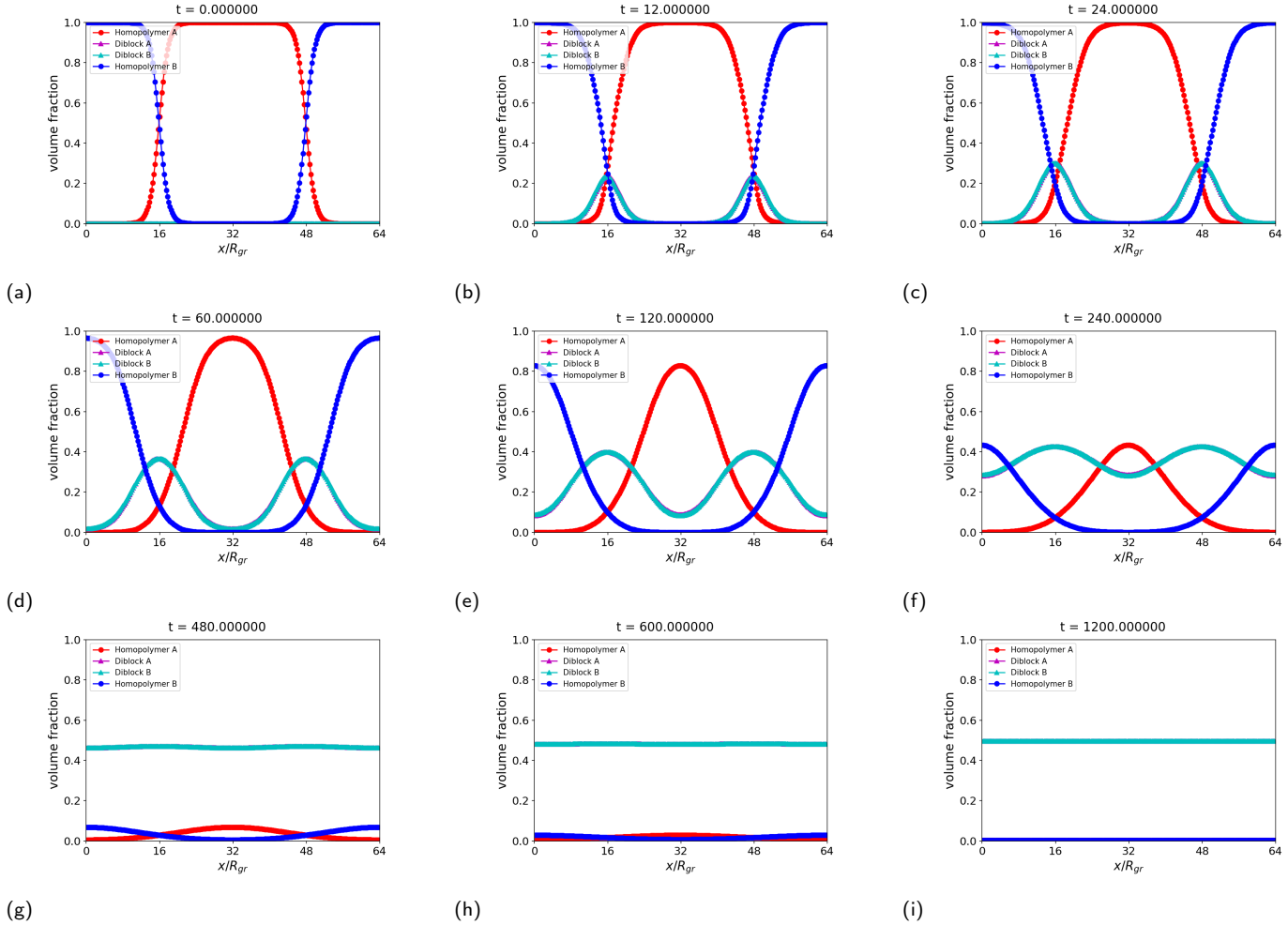

Fig. 4 Time evolution of volume fraction evolutions for a symmetric homopolymer blend undergoing an irreversible end-coupling reaction for $Da_f = 0.3$, and $\chi N_r = 3$. The copolymer builds up at the interface between the two homopolymers and diffuses into the bulk phases. As the homopolymer is slowly depleted, the system undergoes a phase transition into a DIS state.

long times, the relative copolymer concentration in the bulk domains increases to the point that the bulk regions also undergo microphase separation and the system enters the LAM phase and fully transforms into pure copolymer.

Figure 7 shows the reaction rate and interfacial excess for $\chi N_r = 6$. The reaction rate exhibits the initial kinetic limited rate as before. As the system enters the 3φ regime, the reaction rate shows a slight increase when the homopolymer gets entrained in the lamellae and changes slope in Figure 7a. Eventually as the system enters the LAM phase, the reaction rate changes slope again and continues to drop further as the homopolymer is depleted.

The interfacial excess shown in Figure 7b exhibits three regimes as predicted by Fredrickson and Milner [6]. At short times, we see a linear regime (I) representing the kinetically limited reaction. This is followed by a slow increase corresponding to the diffusion limited regime (II). The transition from 2φ to 3φ, indicated by the first enhancement in the reaction rate, occurs here. As the copolymer builds at the interface, the interfacial excess nearly plateaus into the third regime (III) where the copolymer brush presents a strong barrier to homopolymer diffusion. Finally, the interfacial increases peaks slightly as the bulk homopolymer domains start to disappear and the system gradually transitions into the LAM phase. This increase corresponds to the second transition in the reaction rate. The interfacial excess drops dramatically upon the transition and can no longer be calculated once bulk macrophases disappear.

The scaling relations for the rate of copolymer generation based on the morphological state of the system are summarized in Figure 8. Four configurations are considered based on the phase diagram in Figure 1 and the results we have encountered so far: 2φ, 3φ, LAM, and the homogeneous DIS phase. In the 2φ and 3φ phases, contact between the homopolymers occurs only in the interfacial region and the LAM phase, respectively, and the copolymer generation is limited to those regions. Consequently the rate of change of mean copolymer concentration varies proportionally with the width of the interface (ξ) and the thickness of the LAM phase (L_{LAM}), respectively, and inversely with the system size L. While we have studied only one dimensional distributions so far, this suggests that in higher dimensions, the reaction rate in 2φ and 3φ configurations should be proportional to the interfacial area between the homopolymer phases and inversely propor-

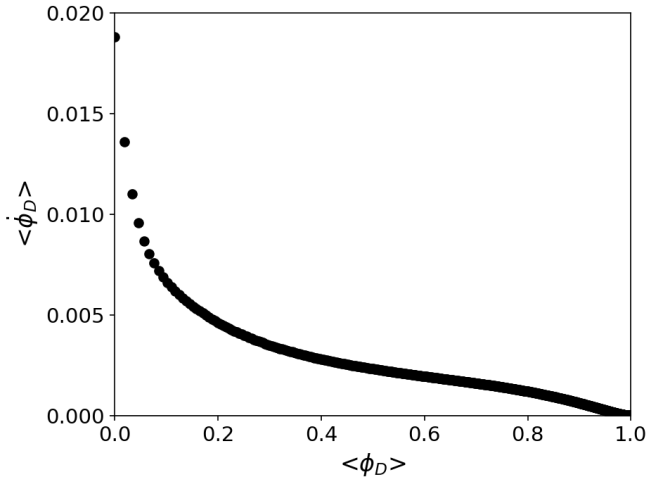

(a) reaction rate

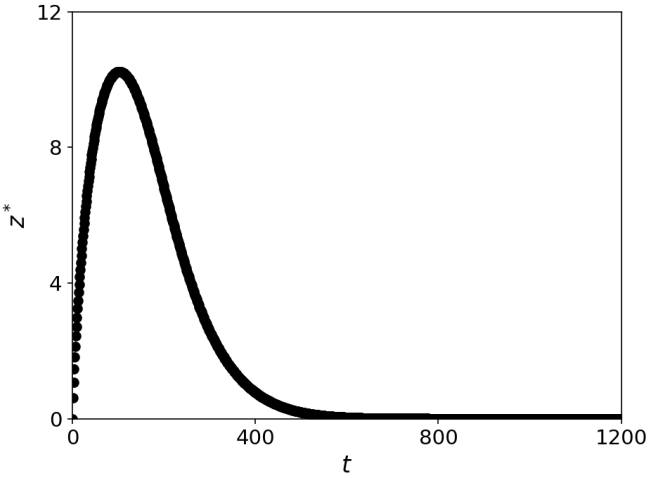

(b) interfacial excess

Fig. 5 Reaction rate vs. volume average diblock concentration (top), and interfacial excess vs. time (bottom) for homopolymer blend simulations shown in Figure 4. The reaction transitions from an initial kinetically limited rate into an eventual diffusion limited rate.

tional to the system volume. In other words, the relevant system size L at higher dimensions is the ratio of volume to interfacial area between the homopolymer macrophases.

The kinetic scaling relations for the LAM and DIS phase do not depend on length scales. For the DIS phase, this is easy to see: the concentrations of all phases are uniform and the reaction occurs over the full system. In the case of the LAM phase, the homopolymers are trapped in the lamellae of the diblock. The reaction occurs over the size of the lamellae. Due to the diffuse nature of the mass distribution over the lamellae, the reaction rate is nearly homogeneous over the macroscopic system and the scaling law does not depend on any length scale. It is important to stress that while the scaling laws for the LAM and DIS phases may look identical, the proportionality constants in front of them may be different.

Figures 9 and 10 show the effect of changing the value of Da_f and χN_r on the reaction rate and interfacial excess respectively. In all of these plots, the initial state is the same. An intrinsically faster reaction with a higher Da_f has a more rapid buildup of the copolymer at the interface during the kinetically limited regime. Consequently the peak in the interfacial excess is also higher and occurs earlier in time. The reaction rate also increases in both the kinetic and diffusion-limited regimes, but the enhancement is much higher during the kinetic limited regime where the reaction rate is less affected by diffusion.

In comparison, raising the incompatibility between the polymers slows down the reaction in both the kinetic and diffusion limited regimes. The interface between the homopolymers gets sharper as their segregation strength increases. In the kinetically limited stage, this slows the reaction rate as the reaction occurs over a smaller region. In the diffusion-limited regime, the homopolymer diffusion through the interfacial brush is hindered by the strong enthalpic repulsion between the homopolymer and the opposite block in the copolymer. This behavior is also consistent with the results of Jones *et al.* [25]. As χN_r rises, the interfacial coverage exhibits three regimes with progressively weakening time dependence predicted by Fredrickson and Milner [6]; namely, an initial kinetically limited regime, an intermediate diffusion limited regime, and a final slow barrier-crossing regime.

5.2 Reversible end-coupling

When the end-coupling reaction is reversible with a finite equilibrium constant, the steady state composition depends on the value of the equilibrium constant as well as χN_r. χN_r determines how well the homopolymers and copolymer mix with each other which affects the rate of the copolymer generation. The rate of copolymer dissociation on the other hand depends only on the amount of copolymer generated. As a result when dynamic equilibrium is established, the mixture composition varies with χN_r even at constant K/N_r. As before, we focus on a symmetric blend only.

Figure 11a shows the equilibrium copolymer volume fraction as a function of the equilibrium constant K/N_r and $Da_f = 1$ for various values of χN_r. As the equilibrium constant increases for fixed forward reaction Damkohler number, the mean copolymer volume fraction also increases since the reverse reaction is weaker

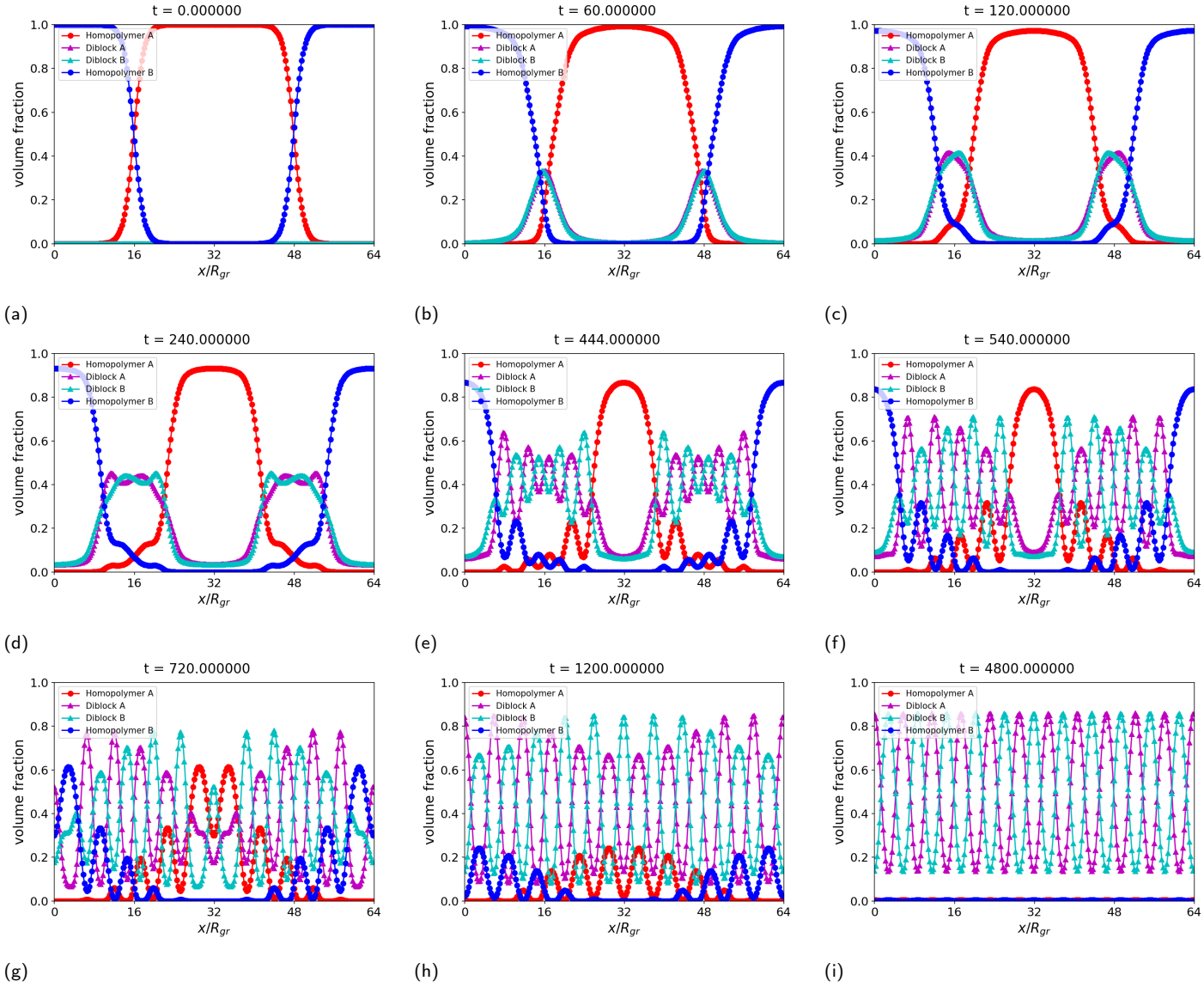

Fig. 6 Time evolution of volume fraction evolution for a symmetric homopolymer blend undergoing an irreversible end-coupling reaction for $Da_f = 0.3$, and $\chi N_r = 6$. As the composition changes, the system transitions from 2φ to 3φ to LAM.

for all χN_r. However as χN_r increases, this rise in copolymer concentration weakens since enthalpic repulsion prevents homopolymer mixing.

The interfacial excess on the other hand has a non-monotonic behavior with K/N_r as shown in Figure 11b. For $\chi N_r = 3$ as the equilibrium constant increases, the reversible reaction favors the formation of the copolymer which builds up at the interface. Above a critical amount of copolymer, the system enters DIS phase. The copolymer concentration becomes homogeneous and the interfacial excess goes to zero by definition. When interfacial excess is zero, the mean copolymer concentration in Figure 11a also follows the analytical result from the DIS phase in Equation 26. At higher χN_r, the interfacial excess increases more slowly with K/N_r. This is also the result of weaker mixing between the homopolymers at higher χN_r. The copolymer is also localized at the interface due to its poor miscibility with the bulk homopolymers, weakening the forward reaction. Consequently the interfacial excess continues to increase until a much higher K/N_r without a transition out of the 2φ region.

Here we also demonstrate the use of scaling relations developed in the previous section to obtain the equilibrium diblock concentration. The relations shown in Figure 8 describe the rate of diblock formation for different morphological configurations. In comparison, the rate of diblock dissociation is easily obtained as

$$\left\langle \dot{\phi}_D \right\rangle = -k_b \left\langle \phi_D \right\rangle \tag{24}$$

At equilibrium, the rates of diblock formation and dissociation are equal. Due to the symmetric nature of the reaction being considered here, the law of mass action may be expressed in terms of the equilibrium constant K and the mean diblock concentration.

For a 2φ system in the Helfand-Tagami limit, we obtain

$$\frac{K}{N_r} = \frac{\langle \phi_D \rangle b}{L\sqrt{6\chi}} \tag{25}$$

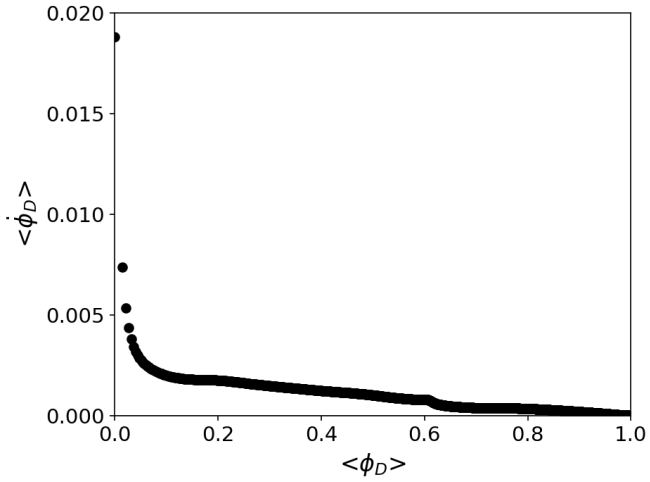

(a) reaction rate

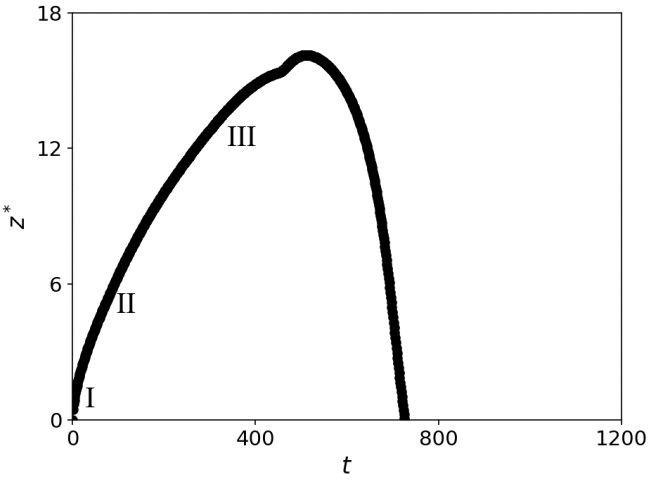

(b) interfacial excess

Fig. 7 Reaction rate vs. extent of reaction (top) and interfacial excess vs. time (bottom) for the homopolymer blend simulation shown in Figure 6. The reaction rate changes slope at each phase transition. The interfacial excess shows increasingly weakening growth rates as the copolymer brush blocks homopolymer diffusion to the interface.

This is shown in Figure 11a in the blue dashed line for $\chi N_r = 8$ and in the inset for $\chi N_r = 6$ in the green dashed line, and matches the simulation results when the equilibrium constant and the amount of copolymer formed are small.

The law of mass action for a fully mixed DIS system can be obtained as,

$$\frac{K}{N_r} = \frac{2\langle\phi_D\rangle}{(1-\langle\phi_D\rangle)^2} \tag{26}$$

This is shown in Figure 11a in the black solid line, and matches the results for $\chi N_r = 3$ when the equilibrium constant is large enough to produce sufficient copolymer to stabilize the DIS phase.

When χN_r is large, such as $\chi N_r = 6$, the system enters the LAM phase when the copolymer amount is high. As stated earlier, the scaling relation of the forward reaction in the LAM phase is similar to that of the DIS phase but with a different numerical prefactor. In the inset of Figure 11a, we show the relation,

$$\frac{K}{N_r} = \frac{8\langle\phi_D\rangle}{(1-\langle\phi_D\rangle)^2} \tag{27}$$

in the green dotted line. This relation matches the simulation results when K/N_r is high.

A similar law of mass action may also exist for the 3φ phase. However, for the specific χN_r and K/N_r parameters employed, we were unable to locate conditions for which the system reached dynamic equilibrium in the 3φ region as opposed to progressing all the way to LAM.

5.3 Extension to 2D systems

We will briefly address the extension to 2D systems. Figure 12a shows the reaction rate for three different 2D initial distributions of homopolymer A: a single circle, four circles, and an ellipse with ratio of major axis and minor axis lengths equal to 4. All three distributions are in the 2φ regime and are chosen to have the same overall composition, where homopolymer A is a minority component with an initial volume fraction of $\phi_{Ah} = 0.41$ and $\chi N_r = 6$. The box sizes in units of R_{gr} are (64,64), (64,64) and (128,32) respectively. A 1D distribution with identical composition is also shown for reference. All distributions exhibit an initial kinetically-determined reaction rate, followed by an eventual transport-limited rate. However the actual rates are different. The four circles distribution has a much higher reaction rate on account of its higher interfacial area between the two homopolymer phases. This is followed by the ellipse, which has the next-highest interfacial area. The circle and the 1D distribution have similar reaction rates.

These differences can be scaled out, as shown in Figure 12b, if the reaction rate is multiplied by a characteristic length l. This length is given by the ratio of area to perimeter of each initial 2D distribution. For the 1D distribution, this length corresponds to the length of the homopolymer A phase divided by 2, the number of interfaces between the two homopolymers in the periodic simulation cell. By extension, in 3D, l would be given by the ratio of the volume to the surface area of the homopolymer A phase. The form of this characteristic length scale is explained by the fact that while the reaction occurs at the interface between the

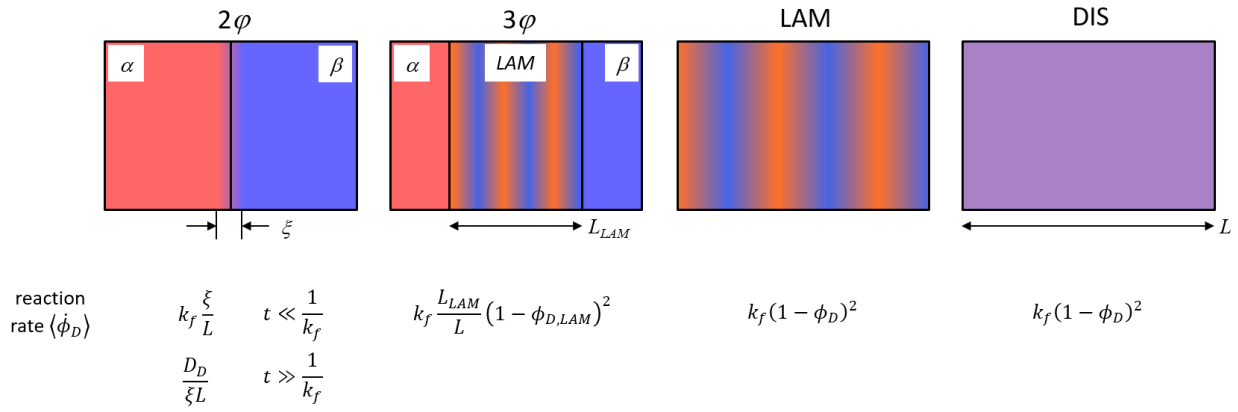

Fig. 8 Scaling relations for the rate of copolymer generation in an irreversibly reactive homopolymer blend based on phase structure

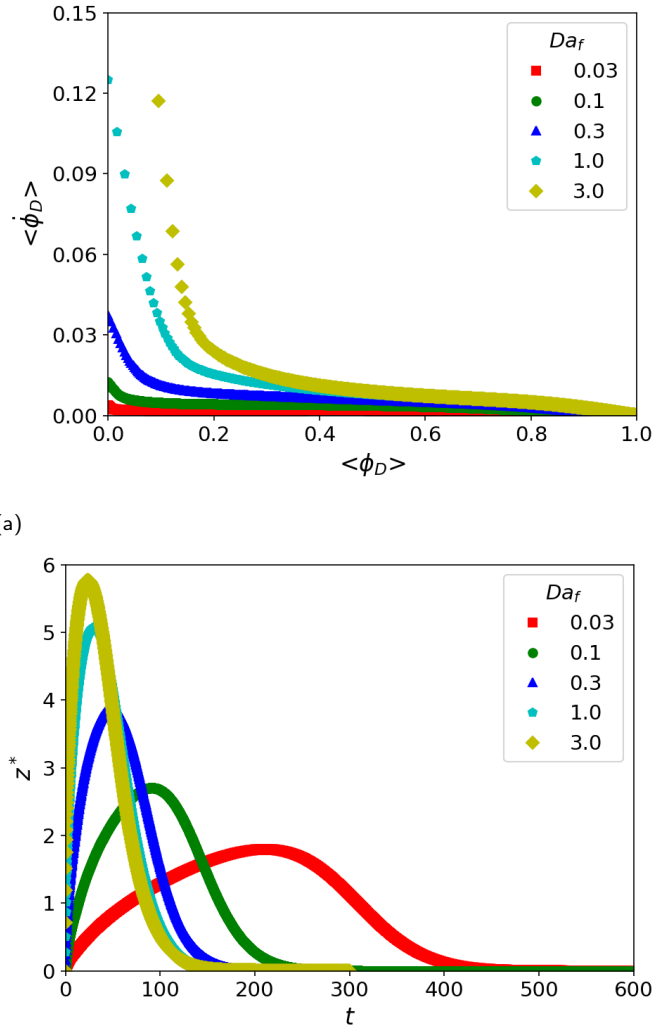

Fig. 9 Reaction kinetics and interfacial excess for a symmetric blend undergoing irreversible reaction with $\chi N_r = 4$ for various values of Da_f. The box size is $32R_{gr}$. The reaction rate increases and the interfacial excess rises faster for higher Da_f.

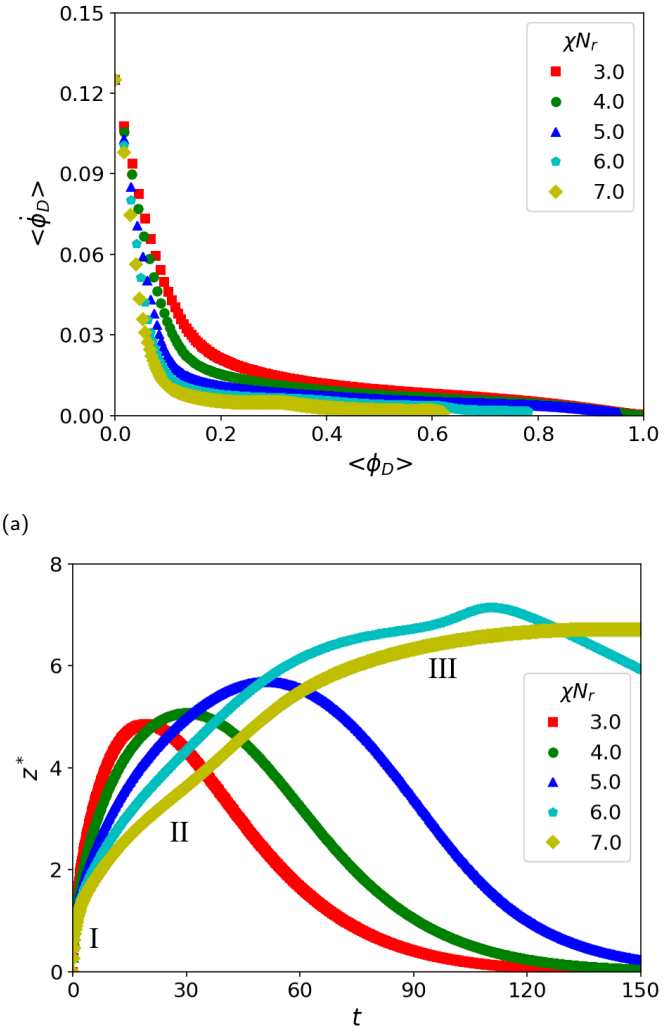

Fig. 10 Reaction kinetics and interfacial excess for a symmetric blend undergoing irreversible reaction with $Da_f = 1$ for varying χN_r with a box size $32R_{gr}$. At higher χN_r, the diffusion of homopolymers to the interface is weaker, resulting in a slower reaction rate.

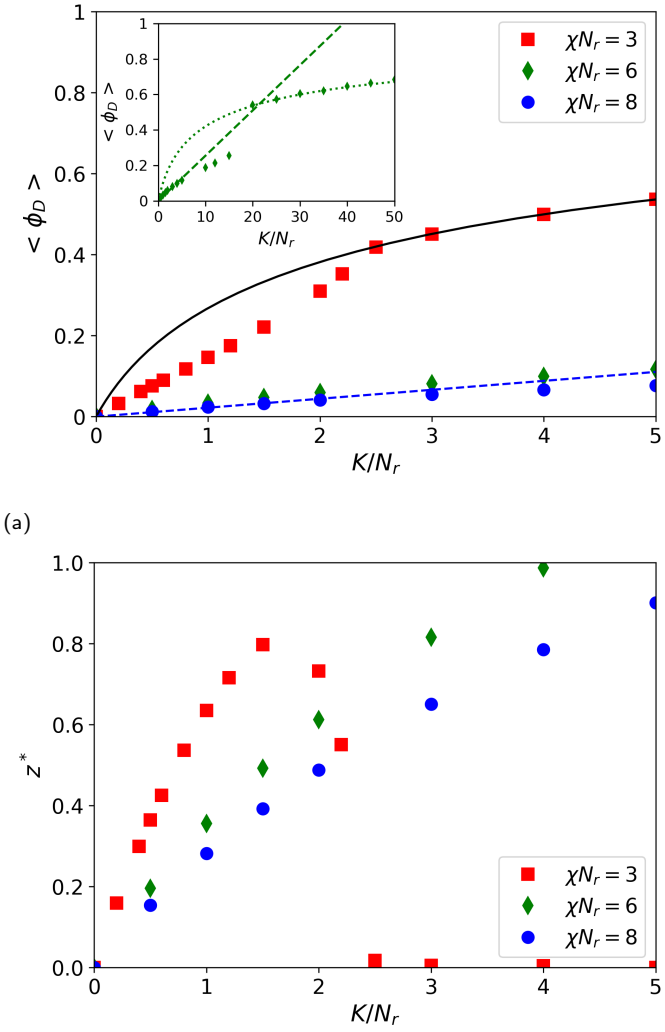

(a)

(b)

Fig. 11 Mean copolymer concentration (top) and interfacial excess (bottom) at equilibrium for a symmetric reversibly reacting blend for varying K/N_r and $Da_f = 1$ with a box size $32R_{gr}$. The solid black line is obtained for a DIS system using Equation 26, while the blue dashed line is obtained for a 2φ system using Equation 25 for $\chi N_r = 8$. The inset shows the mean copolymer concentration for $\chi N_r = 6$ for a wider range of K/N_r. The green dashed line is obtained for a 2φ system using Equation 25 while the green dotted line is obtained for a LAM system using Equation 27.

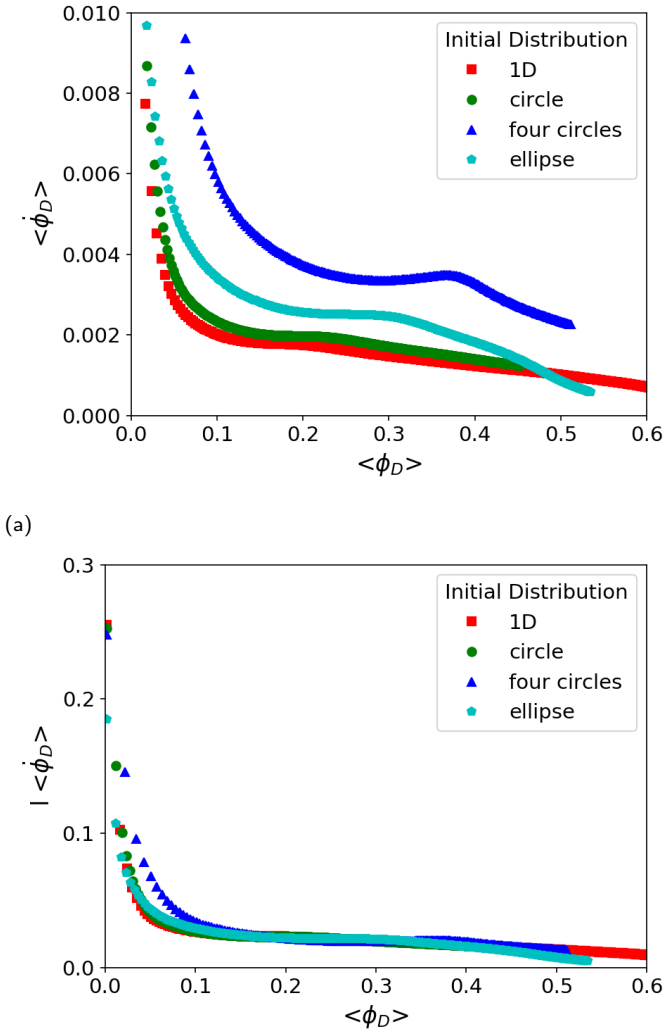

(a)

(b)

Fig. 12 (a) Reaction kinetics for different initial A homopolymer distributions in 2D. (b) The same data re-scaled by a characteristic interface length, l. The reaction rate for different mass distributions collapses when scaled in this way.

homopolymers, the reaction rate is measured in terms of the total volume of each reactant. While the collapse seen in Figure 12b is significant, it is not fully quantitative. This is because the curvature of the interfacial manifold can also influence the reaction rate, which is particularly evident in the four circles case.

Computations in 2D and 3D geometries are also required to study more complex dynamical phenomena associated with reactive blending processes, such as the effect of externally imposed flows and spontaneous emulsification[13]. These, however, merit dedicated analyses and will be addressed in a separate paper.

5.4 Asymmetric blends

Extending the problem to asymmetric blends expands the parameter space significantly and is beyond the scope of this work. However, we will briefly comment on it here. The phase diagram of asymmetric ternary homopolymer-copolymer blends, including

unequal homopolymer chain length and composition, is complex with a rich variety of mesophases and two and three-phase regions[15]. We will address each of these asymmetries separately.

In blends of homopolymers with symmetric chain lengths but unequal concentrations, the blend consists of one homopolymer in excess. In irreversible reactions, the end product consists of a copolymer blended with the excess homopolymer. The reaction kinetics of such a case in 1D is shown in Figure 13a and the corresponding interfacial excesses are shown in Figure 13b. For weakly asymmetric compositions, the reaction kinetics and interfacial excess nearly track the symmetric compositions until the very end when one of the reactants is nearly depleted. As the initial composition becomes more asymmetric, the deviation from the symmetric composition trajectory occurs much earlier. In any case, the initial kinetically-limited and eventual diffusion-limited behavior of the reaction kinetics is retained.

Most polymer blends in practice are also made from homopolymers with unequal chain lengths. In such a situation, a reactively formed copolymer partitions preferentially at equilibrium into the homopolymer with longer chains due to the smaller number of unfavorable A-B contacts. Another important role is played by mixing entropy of unequal length chains, which is demonstrated in Figure 14a showing a *non-reactive* blend of a *symmetric* copolymer with homopolymers of different lengths at equilibrium. The symmetric diblock is seen to be partition into the shorter B homopolymer phase due to mixing entropy. The former type of compatibility-based partitioning is illustrated for an asymmetric diblock mixed with symmetric, non-reactive homopolymers, as seen in Figure 14b.

Perhaps a more important consequence of chain length asymmetry is that, on a volumetric basis, the two homopolymers are consumed by the reaction at different rates. Since one chain of each species reacts in a single instance, the longer polymer is consumed faster than the shorter one. The resulting diblock is also asymmetric. Consequently, both of the above partitioning effects come into play. The confluence of these factors is demonstrated in Figure 15, which shows the reaction rate for an irreversible reaction of an equal volume fraction mixture when $N_{Ah} = 2N_{Bh}$. For reference, the corresponding symmetric blend where $N_{Ah} = N_{Bh}$ with the same N_{Ah} is also provided, which is the result previously shown in Figure 7a. In the asymmetric case, homopolymer A is consumed volumetrically twice as fast as homopolymer B and the end product comprises of an asymmetric diblock with $f_A = 2/3$ blended with unreacted homopolymer B. Additionally, the shorter B homopolymer has a larger concentration of reactive groups and diffuses faster, increasing the reaction rate in both the kinetically and diffusion limited regimes. The interfacial excess also rises faster in the asymmetric blend for the same reason. It is noteworthy that the reaction still retains an initial kinetically limited and an eventual diffusion limited nature.

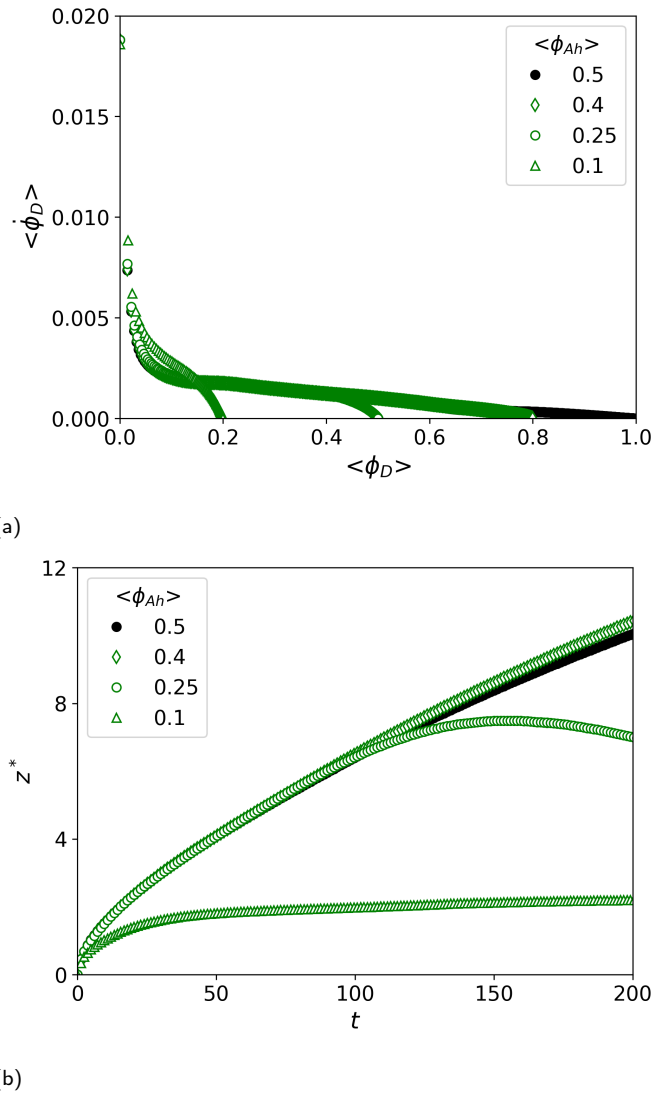

Fig. 13 Reaction kinetics (a) and interfacial excess (b) for an irreversible reaction of homopolymers with symmetric lengths but asymmetric compositions. The labels indicate the initial mean volume fraction of homopolymer A. While the initial kinetically limited and the eventual diffusion limited nature of the reaction is retained, a more asymmetric composition results in faster reactant depletion.

6 Conclusion

We have developed and investigated a dynamic phase field model for reactive end-linking of polymer blends. A density functional type free energy was derived using the procedure of Uneyama and Doi[26]. This free energy functional provides a description of multi-

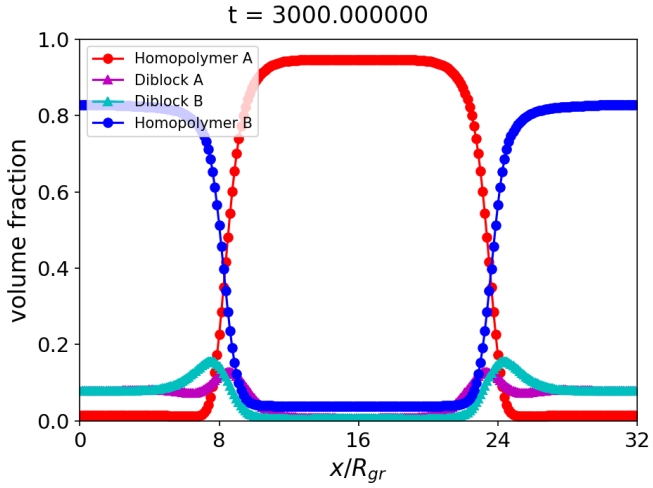

(a)

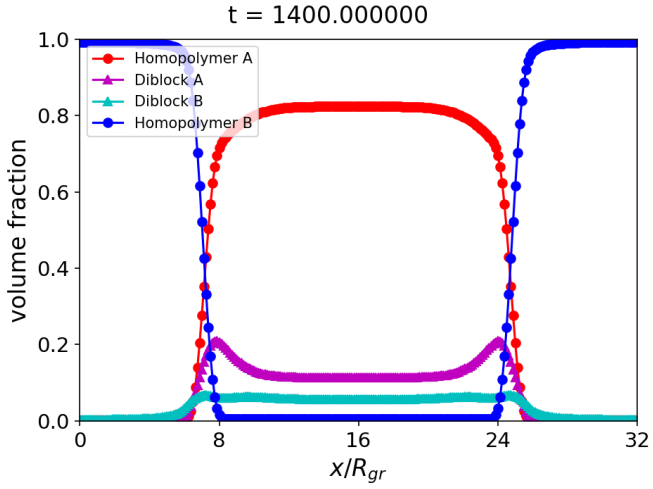

(b)

Fig. 14 Equilibrium volume fraction distributions of non-reacting blends of polymers with asymmetric chain lengths. (a) $N_{Ah} = 2N_{Bh} = N_D/2$, $f = 0.5$ (b) $N_{Ah} = N_{Bh} = N_D/2$, $f = 2/3$. For blends with asymmetric chain architecture, the copolymer partitions into one of the two bulk homopolymer phases.

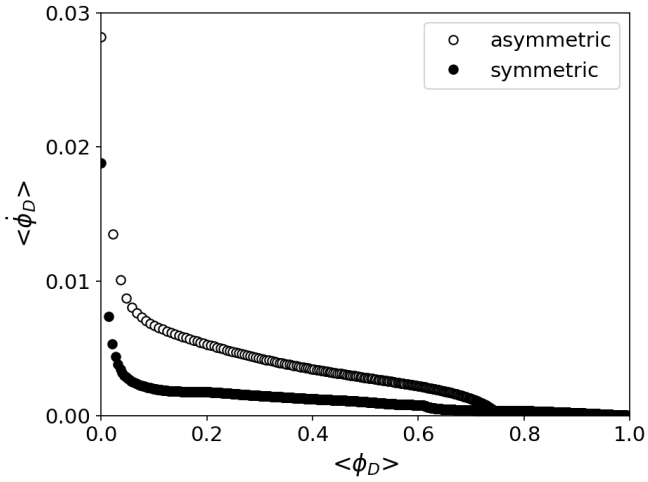

(a) reaction rate

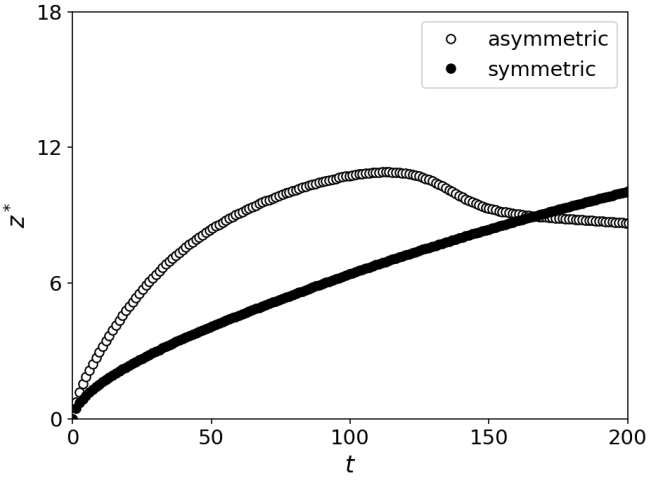

(b) interfacial excess

Fig. 15 Reaction rate and interfacial excess for an irreversibly reacting homopolymer blend with asymmetric chain lengths $N_{Ah} = 2N_{Bh}$ but symmetric composition. A fully symmetric blend, $N_{Ah} = N_{Bh}$, with the same N_{Ah} is shown for reference.

component self-assembly and phase behavior that is shown to yield semi-quantitative agreement with self-consistent field theory (SCFT). For a symmetric blend, this amounts to a well-mixed DIS structure below the Flory incompatibility and at high copolymer content below the Leibler incompatibility, a 2φ coexistence at low copolymer content above the Flory incompatibility, and 3φ coexistance and a LAM phase at intermediate copolymer content and above the Lifshitz incompatibility. The dynamic simulations also show that the reaction progresses through an initial kinetically limited regime and an eventual diffusion-limited regime as previously known[6]. In the 3φ region, the homopolymer is entrained within the lamellae of the diblock-rich phase, extending the reaction manifold and slightly increasing the reaction rate. This enhanced reaction rate scales proportionally to the thickness of the LAM phase relative to the total system size.

We have identified scaling laws for the rate of irreversible end-coupling in each of the four different morphologies. We find that the rate of copolymer formation for the 2φ and 3φ phases depends on the interfacial width and system size. The result for the 2φ phase is in agreement with the literature[11]. In contrast, the scaling laws for the DIS and LAM phases do not depend on the system size, because the reactants are largely well-mixed in both these phases. Furthermore, we find that these scaling laws can be used to predict the equilibrium composition of a reversibly reacting blend when combined with an appropriate reaction model for copolymer dissociation.

For irreversibly reacting systems in the kinetically limited regime, the scaling law depends on the interfacial area to volume ratio and rates can be calculated if the microstructure of the blend is known. By the same token, the reaction rate can be enhanced by increasing the interfacial area, which is achieved in practice by mixing the homopolymers using active or passive mixers. Over time, the copolymer product builds up at the interface and prevents contact between the homopolymers, slowing down the reaction. The reaction rate is then controlled by the diffusion of homopolymer chains through the interfacial brush. Mixing flows are expected to improve the reaction rate in this regime by stretching the interface and diluting or destroying the copolymer brush, exposing fresh interface for reaction. An extension of the present model to include convective transport is needed to investigate this phenomenon in depth.

In summary, the present model and simulations provide a rich description of the complex interplay between thermodynamics, diffusive transport, and reaction kinetics in reactive blending of polymers. The mathematical framework is flexible enough to allow for extensions to study more complex phenomena such as spontaneous emulsification and the effect of externally imposed flows. We look forward to reporting on future investigations of these topics.

Acknowledgements

M.T. was supported by DSM N.V. K.T.D. and G.H.F. were partially supported by the National Science Foundation Grant Nos. DMR-1822215 and DMR-2104255. Simulations were performed using computational facilities purchased with funds from the National Science Foundation (CNS-1725797) and administered by the Center for Scientific Computing (CSC). The CSC is supported by the California NanoSystems Institute and the Materials Research Science and Engineering Center (MRSEC; NSF DMR-1720256) at UC Santa Barbara.

Notes and references

1 C. W. Macosko, H. K. Jeon and T. R. Hoye, *Progress in Polymer Science*, 2005, **30**, 939 – 947.
2 C. Koning, M. V. Duin, C. Pagnoulle and R. Jerome, *Progress in Polymer Science*, 1998, **23**, 707 – 757.
3 H. Pernot, M. Baumert, F. Court and L. Leibler, *Nature Materials*, 2002, **1**, 54–58.
4 H. T. Oyama, R. Nakayama, K. Takase and M. Furuta, *Polymer*, 2018, **137**, 107 – 111.
5 L. Wang, W. Ma, R. Gross and S. McCarthy, *Polymer Degradation and Stability*, 1998, **59**, 161 – 168.
6 G. H. Fredrickson and S. T. Milner, *Macromolecules*, 1996, **29**, 7386–7390.
7 M. Prusty, *PhD thesis*, Technische Universiteit Eindhoven, Department of Chemical Engineering and Chemistry, 2006.
8 J. M. Eagan, J. Xu, R. Di Girolamo, C. M. Thurber, C. W. Macosko, A. M. LaPointe, F. S. Bates and G. W. Coates, *Science*, 2017, **355**, 814–816.
9 S. T. Milner and H. Xi, *Journal of Rheology*, 1996, **40**, 663–687.
10 U. Sundararaj and C. W. Macosko, *Macromolecules*, 1995, **28**, 2647–2657.
11 B. O'Shaughnessy and U. Sawhney, *Phys. Rev. Lett.*, 1996, **76**, 3444–3447.
12 S.-P. Lyu, J. J. Cernohous, F. S. Bates and C. W. Macosko, *Macromolecules*, 1999, **32**, 106–110.
13 J. Jiao, E. Kramer, S. de Vos, M. Möller and C. Koning, *Polymer*, 1999, **40**, 3585–3588.
14 P. K. Janert and M. Schick, *Macromolecules*, 1998, **31**, 1109–1113.
15 P. K. Janert and M. Schick, *Macromolecules*, 1997, **30**, 137–144.
16 F. S. Bates, W. W. Maurer, P. M. Lipic, M. A. Hillmyer, K. Almdal, K. Mortensen, G. H. Fredrickson and T. P. Lodge, *Phys. Rev. Lett.*, 1997, **79**, 849–852.
17 D. Düchs, V. Ganesan, G. H. Fredrickson and F. Schmid, *Macromolecules*, 2003, **36**, 9237–9248.
18 T. L. Morkved, B. R. Chapman, F. S. Bates, T. P. Lodge, P. Stepanek and K. Almdal, *Faraday Discuss.*, 1999, **112**, 335–350.
19 B. Vorselaars, R. K. W. Spencer and M. W. Matsen, *Phys. Rev. Lett.*, 2020, **125**, 117801.
20 D. Broseta and G. H. Fredrickson, *The Journal of Chemical Physics*, 1990, **93**, 2927–2938.
21 E. H. Feng, W. B. Lee and G. H. Fredrickson, *Macromolecules*, 2007, **40**, 693–702.
22 J. S. Schulze, J. J. Cernohous, A. Hirao, T. P. Lodge and C. W. Macosko, *Macromolecules*, 2000, **33**, 1191–1198.
23 P. Guegan, C. W. Macosko, T. Ishizone, A. Hirao and S. Naka-

hama, *Macromolecules*, 1994, **27**, 4993–4997.
24 C. Scott and C. Macosko, *Journal of Polymer Science Part B: Polymer Physics*, 1994, **32**, 205–213.
25 T. D. Jones, J. S. Schulze, C. W. Macosko and T. P. Lodge, *Macromolecules*, 2003, **36**, 7212–7219.
26 T. Uneyama and M. Doi, *Macromolecules*, 2005, **38**, 196–205.
27 J. V. Liu, C. J. García-Cervera, K. T. Delaney and G. H. Fredrickson, *Macromolecules*, 2019, **52**, 2878–2888.
28 V. V. Khatavkar, P. D. Anderson, P. C. Duineveld and H. H. E. Meijer, *Macromolecular Rapid Communications*, 2005, **26**, 298–303.
29 N. Jaensson, M. Hulsen and P. Anderson, *Computers and Fluids*, 2017, **156**, 81 – 96.
30 P. C. Hohenberg and B. I. Halperin, *Rev. Mod. Phys.*, 1977, **49**, 435–479.
31 M. Doi and A. Onuki, *J. Phys. II France*, 1992, **2**, 1631–1656.
32 M. Cromer, M. C. Villet, G. H. Fredrickson and L. G. Leal, *Physics of Fluids*, 2013, **25**, 051703.
33 J. D. Peterson, M. Cromer, G. H. Fredrickson and L. G. Leal, *Journal of Rheology*, 2016, **60**, 927–951.
34 J. D. Peterson, G. H. Fredrickson and L. G. Leal, *Journal of Rheology*, 2019, **63**, 335–359.
35 D. R. Tree, K. T. Delaney, H. D. Ceniceros, T. Iwama and G. H. Fredrickson, *Soft Matter*, 2017, **13**, 3013–3030.
36 D. R. Tree, T. Iwama, K. T. Delaney, J. Lee and G. H. Fredrickson, *ACS Macro Letters*, 2018, **7**, 582–586.
37 D. R. Tree, L. F. Dos Santos, C. B. Wilson, T. R. Scott, J. U. Garcia and G. H. Fredrickson, *Soft Matter*, 2019, **15**, 4614–4628.
38 G. Fredrickson, *The Equilibrium Theory of Inhomogeneous Polymers*, 2005.
39 M. W. Matsen and M. Schick, *Current Opinion in Colloid and Interface Science*, 1996, **1**, 329 – 336.
40 R. A. Riggleman and G. H. Fredrickson, *The Journal of Chemical Physics*, 2010, **132**, 024104.
41 L. Leibler, *Macromolecules*, 1980, **13**, 1602–1617.
42 T. Ohta and K. Kawasaki, *Macromolecules*, 1986, **19**, 2621–2632.